LYRA: the Solar UV radiometer aboard the ESA Proba–2 ⋆

J.-F. Hochedez [a,*], W. Schmutz [b], M.Nesladek [c,j], Y. Stockman [d], U. Schühle [e], A. BenMoussa [a], S. Koller [b], K. Haenen [c,j], D. Berghmans [a], J.-M. Defise [d], J.-P Halain [d], A. Theissen [a], V. Delouille [a], V. Slemzin [g], D. Gillotay [f], D. Fussen [f], M. Dominique [f], F. Vanhellemont [f], D. McMullin [h], M. Kretzschmar [i], A. Mitrofanov [g], B. Nicula [a], L. Wauters [a], H. Roth [b], E. Rozanov [b], I. Rüedi [b], C. Wehrli [b], H. Amano [m] R. Van der Linden [a], A. Zhukov [a], F. Clette [a], S. Koizumi [ℓ], V. Mortet [c], Z. Remes [c], R. Petersen [j], M. D'Olieslaeger [c,j], J. Roggen [k], P. Rochus [d],

[a] *Royal Observatory of Belgium (ROB), Circular Avenue 3, B-1180 Brussels, Belgium*

[b] *Physikalisch-Meteorologisches Observatorium Davos (PMOD) and World Radiation Center (WRC), Dorfstrasse 33, CH-7260 Davos Dorf, Switzerland*

[c] *Institute for Materials Research, Limburgs Universitair Centrum, Wetenschapspark 1, B-3590 Diepenbeek, Belgium*

[d] *Centre Spatial de Liège (CSL) - Avenue du Pré Aily B-4031 Angleur - Belgium*

[e] *Max-Planck-Institut für Sonnensystemforschung (MPS) - D-37191 Katlenburg-Lindau - Germany*

[f] *Belgian Institute for Space Aeronomy (BISA), Circular Avenue 3, B-1180 Brussels, Belgium*

[g] *Lebedev Physical Institute (LPI), 53 Leninsky Prospect, Moscow, 119991, Russia*

[h] *Naval Research Laboratory (NRL), 4555 Overlook Avenue, S.W., Washington, DC 20375, USA*

[i] *Istituto Fisica dello Spazio Interplanetario, Consiglio Nazionale delle Ricerche, Via del Fosso del Cavaliere, 100, I-00133 Roma, Italy*

[j] *Division IMOMEC, IMEC vzw, Wetenschapspark 1, B-3590 Diepenbeek, Belgium*

[k] *IMEC, Kapeldreef 75, B-3001 Leuven, Belgium*

[ℓ] *Advanced Materials Laboratory, National Institute for Materials Science (NIMS), 1-1 Namiki, Tsukuba 305-0044, Japan*

[m] *Department of Materials Science and Engineering, Meijo University, 1-501 Shiogamaguchi,Tempaku-ku, Nagoya 468-8502, Japan*

Preprint submitted to Elsevier Science *22 October 2004*

Abstract

LYRA is the solar UV radiometer that will embark in 2006 aboard Proba–2, a technologically oriented ESA micro-mission. LYRA is designed and manufactured by a Belgian–Swiss–German consortium (ROB, PMOD/WRC, IMOMEC, CSL, MPS & BISA) with additional international collaborations. It will monitor the solar irradiance in 4 UV passbands. The channels have been chosen for their relevance to Solar Physics, Aeronomy, and Space Weather: 1/ 115-125 nm (Lyman–α), 2/ the 200–220 nm Herzberg continuum range, 3/ Aluminium filter channel (17–30 nm) including He II at 30.4 nm, and 4/ Zirconium filter channel (1–20 nm). The radiometric calibration will be traceable to synchrotron source standards (PTB & NIST), and the stability will be monitored by on-board calibration sources (VIS & NUV LEDs). These allow to distinguish between possible degradations of the detectors and filters. Additionally, a redundancy strategy maximizes the accuracy and the stability of the measurements. LYRA will benefit from wide bandgap detectors based on diamond: it will be the first space assessment of a pioneering UV detectors program. Diamond sensors make the instruments radiation-hard and solar-blind: their high bandgap energy makes them insensitive to visible light and, thus, make dispensable visible light blocking filters, which seriously attenuate the desired ultraviolet signal. Their elimination augments the effective area, and hence the signal-to-noise, therefore increasing the precision and the cadence. The SWAP EUV imaging telescope will operate next to LYRA on Proba–2. Together, they will establish a high performance solar monitor for operational space weather nowcasting and research. LYRA demonstrates technologies important for future missions such as the ESA Solar Orbiter.

Key words: Sun: Irradiance, Sun: UV radiation, Sun: flares, solar-terrestrial relations, Aeronomy, Instrumentation: detectors, Diamond, Techniques: Radiometry
PACS: 78.20.-e, 78.40.Fy, 78.66.Db, 85.60.Dw, 94.10.-s, 94.20.-y, 94.80.+g, 07.87.+v, 07.89.+b, 95.55.Ev, 95.55.Qf, 95.75.Wx, 95.85.Mt, 96.60.Rd, 96.60.Tf

1 Introduction

The knowledge of the solar spectral irradiance is of large interest to Solar Physics, Aeronomy, and to other fields of heliospheric or planetary research. The solar ultraviolet (UV) irradiance below 300 nm is the main source of the energy converted in the Earth's atmosphere, controlling its thermal structure,

⋆ http://lyra.oma.be/

* Corresponding author.
Email address: hochedez@oma.be (J.-F. Hochedez).

dynamics and chemistry through photo-dissociation and photo-ionization. Of special interest for life and mankind is the balance of ozone formed by radiation below 240 nm in the stratosphere and mesosphere, but photodissociated above 200 nm in the stratosphere (e.g. Egorova et al., 2004; Rozanov et al., 2004). The VUV irradiance variability has significant effects on human technologies too, currently addressed in the frame of Space Weather studies.

The solar spectral irradiance is a function of both time and wavelength, and one would ideally like to sample it with maximal temporal and spectral resolutions, together with the highest absolute accuracy, precision and time coverage. These quests however encounter physical limits, making them conflicting and imposing trade-offs. The strategy is thus to bridge the most reliable observations, with the best possible models (e.g. Warren et al., 2001; Woods, 2002; Lean et al., 2003).

Numerous experiments are currently monitoring the solar full-disk UV– and X–Ray irradiance. All of them differ in spectral coverage, time coverage, time cadence, and nature of the instrument (spectrograph, photometer, or imager). Some data characterizing these missions are summarized in Table 1. Full-disk spectrographs are used in UARS–SOLSTICE (Solar Stellar Irradiance Comparison Experiment; Rottman et al. (1993); Woods et al. (1993)), in UARS–SUSIM (Solar Ultraviolet Spectral Irradiance Monitor, Vanhoosier et al. (1981); Brueckner et al. (1993)), in SoHO–SEM (Solar EUV Monitor, Judge et al. (1998)), in SORCE–SOLSTICE II, in SORCE–SIM (Spectral Irradiance Monitor), and in TIMED–SEE (Solar EUV Experiment, Woods et al. (1998)). SEE includes XPS, a photometer system, for the short wavelength range, whereas photometer systems are exclusively used in GOES–XRS (X–Ray Sensor) and in SNOE–SXP (Solar X–Ray Photometer, Bailey et al. (2000)).

In principle, more information can be extracted from spectrographs than from photometers such as LYRA, however, under the sacrifice of cadence. Also, not all missions are designed for continuous data aquisition. For instance, measurements with TIMED–SEE are made for only 3 minutes per 97 minute orbit during which the Sun moves per-chance into the field of view. While this is not ideal for the study of phenomena that occur unexpectedly and vary in time, flares have been observed during such short observation periods(Woods et al., 2004). Generally, the required integration times are higher for spectrographs, and time has to be spent on spectral scanning. It all unfavourably affects their time cadence. The SORCE–SOLSTICE experiment allows spectral scans to be restricted to Lyα and Mg II (280 nm), thereby achieving its highest cadence of $\approx$1 minute. Lyα profile variations during flares have been detected that way (Wang et al., 2000; Woods et al., 2004). While this is beyond its scope, LYRA has the advantage of continuous monitoring in the day phase of its orbit. Moreover, it offers the novelty of very high cadence observations down

Table 1
Comparison of LYRA with other current and future solar irradiance experiments

Satellite	Experiment	Spectral range [nm]	type	Nominal freq. of aquisition	time of operation
Proba–2	LYRA	1–20, 17–70 Lyα, 200-220	p	cadence $\geq$ 0.01 s	2006–2008–
Coronas	SPIRIT	30.4, 17.5	i	cadence: 5"–15'	Aug. 2001–
		19.5, 28.4		day: 45', orbit: 93.5'	
Goes	XRS	0.1–0.8, 0.05–0.4	p	cadence 0.5 s	since 1974
	SXI	0.6–6.0	i	cadence 1 min	since 2001
Iss	SolACES	17-220	s	15 spectra per day	2006–2009–
	SOLSPEC	180-3200	s	15 spectra per day	2006–2009–
	SOVIM	310nm–100μm	p	cadence $\geq$ 1 min	2006–2009–
Snoe	SXP	2–7, 6–19, 17–20	p	cadence 62.8 ms, not continuous	03/11/1998 –12/13/2003
Soho	SEM	0.1–50	s	cadence 15 sec	1996–
	EIT	30.4, 17.1,	i	few per day	1996–
		19.5, 28.4			
Sorce	SOLSTICE	115–310	s	at least every 6 h	06/03/2003–
	SIM	200–3000	s	4 times per day	06/03/2003–
	XPS	1–35, Lyα	p		06/03/2003–
Timed	SEE	0.1–195	s+p	cadence 10 s not continuous	22/01/2002–
Uars	SOLSTICE	119–420	s		Oct. 1991–
	SUSIM	115–410	s		Oct. 1991–

type: p = photometer, s = spectrograph, i = imager.

to 10 milliseconds, which is of interest for the study of solar flares (Woods et al., 2003; Snow et al., 2004), and for the limb occultation technique (See section 3.3). The maximum cadence of LYRA is higher than the one of SNOE–SXP, an instrument widely used for atmospheric studies and similar to LYRA except that it lacks longer wavelength channels at Lyα and at the Herzberg continuum. Also, SXP does not monitor the Sun in a continuous fashion. Continuous long-term time series of the EUV solar irradiance can bring insights into fundamental questions such as coronal heating (Greenhough et al., 2003), but here also, the higher the sampling rate, the less the bias of the statistics.

Full-disk imagers such as EIT (EUV Imaging Telescope) on SOHO, SPIRIT on CORONAS, SXT (Soft X–Ray Telescope) on YOHKOH, or SXI (Solar X–Ray Imager) on the GOES series of satellites enable irradiance measurements with the additional (and actually primary) benefit of spatial resolution (Newmark

et al., 2001). Sub-second cadence, however, is not yet achieved.

Further future instruments measuring solar UV– and X–Ray irradiances are SolACES (Solar Auto-Calibrating EUV/UV Spectrophotometers), SOVIM (Solar Variability and Irradiance Monitor), SOLSPEC (Solar Spectrum Measurement Instrument) onboard the International Space Station (ISS), and EVE (EUV Variability Experiment) aboard SDO. There is no guarantee though that there will be no gap in the future regarding the time–wavelength coverage.

Of maximum benefit for astrophysical and atmospherical studies is the combination of data of complementary instruments. Spectrographs, imagers and photometers are all designed for their specific purposes, and LYRA will add sub-second cadence capabilities to the currently available ensemble of solar irradiance experiments.

This paper describes LYRA (the LYman–α RAdiometer), a solar VUV photometer, and the preparation to exploitation of its observations. One purpose of the instrument is to demonstrate several technologies able to enhance vacuum ultraviolet measurements by increasing the overall effective area, and the ability to maintain calibration. The former feature permits a better precision versus cadence trade-off, the latter, a higher accuracy. LYRA will benefit from diamond detectors: it will be the first space assessment of a pioneering UV detectors program (Hochedez et al., 2000, 2001, 2002, 2003a,b; Schühle et al., 2004).

2 Instrument description

LYRA is part of the Proba–2 (Project for On-board Autonomy) space mission of the European Space Agency (ESA), which aims at demonstrating technologies embedded in its technical or scientific payload. Proba–2 is a follow-up of the successful Proba–1 program in orbit since October 2001 (Teston et al., 1999). It includes major Belgian contributions. It is developed under an ESA General Support Technology Program (GSTP) contract by a consortium led by Verhaert Design & Development (Belgium). It will be launched as a piggy back payload, to reach a heliosynchronous polar orbit stabilized at 10:30 for a 2-year mission.

Beyond LYRA, the Proba–2 Science payload contains the Thermal Plasma Measurement Unit and the Dual Segmented Langmuir Probe for Space environment, and SWAP (Sun Watcher using an Active Pixel Sensor and image Processing; Defise et al. (2004); Berghmans (2005)). LYRA and SWAP teams emphasize their synergies for fundamental scientific research, and operational

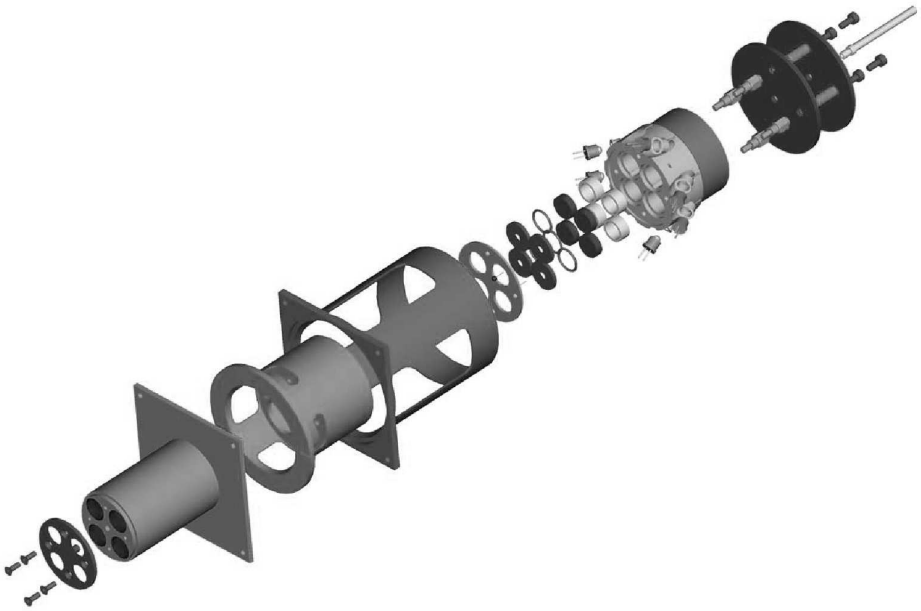

Fig. 1. Exploded view of one of the three identical LYRA units. The collimator, the filters, the LEDs and the head can be seen. The detectors are hidden by the head.

Space Weather nowcast/forecast.

2.1 Radiometer design

LYRA is a compact solar VUV radiometer, designed, manufactured and calibrated by a Belgian–Swiss–German consortium with additional international collaborations. It encompasses three redundant units including four spectral channels each: 1–20 nm (Zr), 17–30 nm (Al), 115-125 nm (Lyα) and 200–220 nm (Herzberg). Each channel consists in a collimator and a head with a precision aperture, a spectral filter, a detector and two LED light sources (See Fig. 1). The Physikalisch Meteorologisches Observatorium Davos (PMOD, Swizterland) provides the optical–, electronical– and mechanical design. The solar-blind diamond detectors have been designed and fabricated at IMOMEC, Belgium with the collaboration of the National Institute for Materials Science (NIMS), Tsukuba, Japan. The LYRA development takes into account cleanliness and thermal issues. Despite a non-optimal orbit, limited platform resources, and only 16 months of development, LYRA will normally be delivered to the platform in time (spring 2005).

The dimensions of LYRA are 315 mm × 92.5 mm × 222 mm, and its weight is 5.0 kg. Given the geometry of the collimator, view-limiting apertures of 8 mm diameter, precision apertures of 3 mm diameter, and detector sensitive area

Table 2
Expected signal and spectral purity for generic detectors (PiN for Herzberg, MSM otherwise)

LYRA Channel	purity definition	Active Sun	Purity	Solar Min	Purity
Herzberg	200–220 nm	12.2 nA	87.0 %	12.2 nA	87.0 %
Lyman–α	121.6 ± 2.5 nm	55.4 pA	73.6 %	37.0 pA	63.3 %
Al	HeII (30.5 ± 1.25 nm)	1.4 nA	53.5 %	355 pA	56.2 %
Zr	0–20 nm	671.3 pA	99.4 %	135 pA	99.4 %

of 4 mm, the unobstructed FOV is 2.06^o and the full opening angle is 4.69^o. Provisions have been taken for mounting tolerances, off-points, and spacecraft jitter.

2.2 Filters, definition of channels, and radiometric model

The two detector types built for LYRA are a photoresistive device (metal-semiconductor-metal junction, MSM) and a pin Schottky type junction (PiN). A radiometric model based on the solar spectral irradiance, transmittance of the LYRA filters, and detector responsivity (PiN and MSM) is used to determine the anticipated photocurrents and their spectral purity. The accuracy of the current draft calculations is not well determined; some approximations such as the extrapolation towards the infrared of the absolute transmittance of interference filters were made. A generic detector was used until all flight model devices were calibrated across the full necessary range. Updating the radiometric model with the most reliable data is a permanent process within the LYRA project. To assess the signal currents and spectral purity, we have summarized both detector types from median responsivity graphs. Table 2 shows the results based on the generic MSM and PiN devices. There is no special difficulty with the Herzberg channel thanks to the relatively large signal expected (> nA). However this must be moderated by the small variability (<2 %), and hence the need for high precision measurement. For Lyman–α, Al and Zr channels, the results based on the generic MSM anticipate a lack of signal with these channels. For the Al and Zr channels the above is alleviated by the relatively large fluctuation expected. As to Lyα, the diamond detectors perform almost as well as an AXUV diode (commercially available reference detector from IRD, based on Si technolgy), which would have implied an additional filter, and its associated concerns, to reach 72.9 pA with 84.8 % purity.

Porous filters specially designed and manufactured by the Lebedev Physical Institut (Russia) are available for LYRA. They have a very high porosity (>20%) making them transmittive in the XUV-EUV. Details of the principle

and fabrication procedure can be found in Mitrofanov and Apel (1989), and following papers. A special effort was made to decrease the size of the pore in order to better reject the VIS and the NUV. A positive decision on a porous filter channel for LYRA is pending a measurement of the actual transmittance in the 1–50 nm range.

2.3 Diamond Detectors and LEDs

Diamond, a wide bandgap material, makes the sensors radiation-hard and 'solar-blind', which makes dispensable filters that block the unwanted visible, but attenuate seriously the desired UV radiation. Two types of diamond detectors are investigated with LYRA: PiN (photodiode) and MSM (photoresistor) structures. PiN devices are intended for the Herzberg (Zr is TBC) channel(s) because they promise maximal solar-blindness, that improves the spectral purity feature. For a channel using thin metallic filters, maximal solar-blindness helps if few pinholes appear. Although MSM devices are less solar-blind and less linear than PiN diodes, they are foreseen for the Lyman–α, Al, and perhaps Zr channels, in order to maximise their effective area.

2.3.1 PiN detectors

P-i-N detector structures were developed in a joint collaboration between IMOMEC and NIMS (Koizumi et al., 2001). The homoepitaxial layers of the detector were deposited in two different ULVAC stainless steel chamber plasma-enhanced microwave deposition reactors. Each apparatus is solely used for one type of doping, i.e. p-type (B) or n-type (P), in order to avoid unwanted contaminations of the CVD diamond layers. After a careful selection and chemical oxidation of {111}-oriented, 5 mm in diameter, 0.5 mm thick, HPHT Ib substrates from Element Six, an epitaxial p-type B-doped layer is deposited. Boron-doping is accomplished by adding trimethylboron (TMB) to the typical low-concentration methane-to-hydrogen mixture of 0.05%. The TMB-to-methane ratio was varied between 100 and 4000 ppm. Other typical process parameters are a pressure of 100 Torr, a substrate temperature around 900–950^{o}C and a microwave power of about 400 W. The intrinsic and P-doped n-type layer are grown in the same deposition run making use of the second growth apparatus. Starting with a normal H_2/CH_4 mixture for the intrinsic layer, phosphine (PH_3) is added after a certain amount of time to get an n-type layer. Compared to the first process, these layers are deposited at a slightly higher microwave power (700 W) and lower substrate temperature (870–900^{o}C), while the PH_3/CH_4 ratio is about 5000 ppm for the n-type layer. In order to make an electrical contact to the B-doped layer, part of the intrinsic/P-doped layer needs to be removed using reactive ion etching (RIE).

Fig. 2. Photograph of a LYRA MSM detector

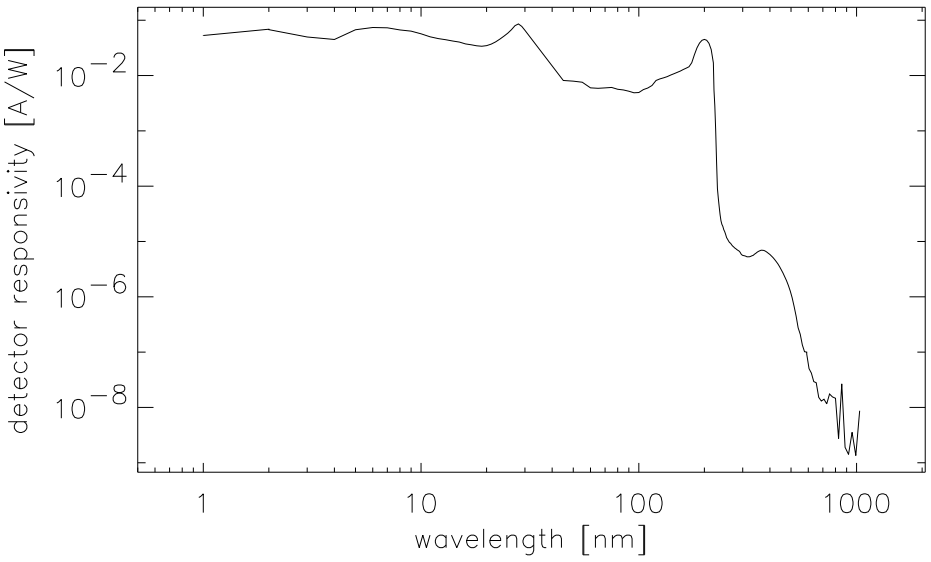

Fig. 3. Responsivity in A/W of the generic MSM detector

Therefore a circular Al film (4.5 mm in diameter) is deposited on top of the structure. This layer, acting as a mask during the RIE, is chemically removed afterwards. As a last step, two ohmic contacts are evaporated. For the p-type layer this is Ti/Al (50/50 nm) ring, while a thin Al layer with a transmittance of typically 20-50 % acts as top contact.

2.3.2 MSM detector

Fabrication of a new circular MSM photodetector using a Ti/Pt/Au multilayer structure for the interdigitated electrodes was carried out at IMO–IMOMEC. A 0.8 μ thick diamond layer was grown epitaxially on single IIa (natural) diamond substrates (500 μm thickness), also from Element Six, using microwave–

plasma enhanced chemical vapor deposition (MECVD) technology. Details of the growth procedure can be found in Remes et al. (2005). The optimisation of the circular contact geometry was done by Garching Analytics GmbH in Germany. A MSM detector is shown in Fig. 2 with its rectangular ceramic (Al_20_3) package. This packaging (not commercially available) has the same dimensions as the Hamamatsu S1337–66BQ. A metal ring contact on the perimeter of the mesa defines the active area of the MSM photodetector, which has an inner diameter of 4.2 mm, corresponding to an optical detection area of 13.9 mm^2.

2.4 Calibrations

2.4.1 Traceability to radiometric standards

It is a scientific goal of LYRA to improve the absolute accuracy of the measurement (goal 5%); hence the need for sub-systems and system calibrations, on-ground and in-flight. The radiometric responsivity of each LYRA channel has to be determined over a wavelength range that is extremely large: from the soft X–Rays (1 nm) to the near infrared. First, subsystems (filters, MSM detectors, PIN detectors) are characterized for their UV responsivity, visible light blocking and suppression, background noise, dark current, temporal stability within different wavelength ranges. Second, the LYRA instrument will be calibrated, each channel separately, consisting of a precision aperture, filter, and detector. The measurements are being carried out by several teams at radiometric calibration facilities who are in collaboration with the LYRA project: CSL, PTB/BESSY, NIST, IMOMEC... To cover such a large spectral range, synchrotron beamline facilities are required. They also provide the traceability to a primary source standard. The calibration results obtained with the different detector types and filters will be reported in a dedicated publication. The global calibration of the LYRA instrument is foreseen in 2005 at the calibration beamline for detector radiometry of the Physikalisch-Technische Bundesanstalt at the electron storage ring BESSY II in Berlin.

Started in November 2003, the pre-delivery test and calibration activities, are expected to finish in Spring 2005 (covering a period of 15 months). The LYRA calibration plan consists of the following calibration programs:

(1) First detector campaign at IMOMEC and PTB/BESSY. This campaign was used to characterize and compare the spectral responsivity of MSM and PiN structures over the spectral range from 40 nm to 240nm (Ben Moussa et al., 2004).
(2) Precision aperture area measurement at PMOD. Only the precision aperture are critical, thus calibrated. The open aperture diameter is 3.0 mm. The manufacturing tolerance of the precision apertures is H7, or +10/-

0 μm in diameter. After manufacturing, the apertures will be sent to the Swiss Federal Office of Metrology and Accreditation (METAS) for calibration. The inspection of roundness allows area calibration by diameter. The overall accuracy must be considered as not better than 1.2 μm in diameter, that is 8.10^{-4} in relative terms.

(3) LEDs calibration campaign at the Amano Laboratory and at IMO. The emissivity of the diodes are tested by calibrated detectors. Reliability tests are also carried out versus prolonged duration, and temperature stress. Finally, the LEDS are tested with the LYRA calibrated detectors.
(4) Filters calibration campaign at CSL, MPS and PTB/BESSY. Measurements of the light transmission is performed. The flight filters are documented with a complete package of certifications. After calibrations, the filters will be mounted on the Flight Model (FM) instrument for vibration, thermal and possible irradiation tests. After these tests, a recalibration of the filters will be done by ARC (Acton Research Corp., USA) for the Lyα and the Herzberg filters, and by PTB/BESSY for the Aluminium and Zirconium filters.
(5) Second detector campaign at IMOMEC, CSL, MPS, NIST and PTB/BESSY. This calibration program of FM–detectors is designed to know their XUV-to-VIS response, and the stability of their performance with time (Ben Moussa et al, 2005). Part of this campaign addresses other characterizations (linearity, flat-field).
(6) Global instrument calibration campaign at PTB/BESSY. This program will assess the radiometric performance of the whole LYRA in order to provide the most accurate knowledge of its spectral response with the flight electronics configuration.

After delivery and during flight operations, further ground calibrations will occur on the LYRA 'calibration head' that is intended to be identical to the FM ones.

2.4.2 In–flight calibration

The redundancy strategy requires that all three units are made as similar as possible. One is used continuously, the second on a weekly basis, while the other remains closed most of the time, and is only used a few times during the mission. In this way, the radiometric evolution of the sensors and filters will be assessed. Furthermore, the LEDs will help disentangle filters and detectors aging, and in-flight flat-field campaigns will look for unexpected burn-in effects.

2.5 Onboard software and operations

The Proba–2 mission is about autonomous operations. LYRA's onboard software will compliantly accomplish the needed tasks in a most optimal manner along an orbit. The Science programs will be uploaded daily from the Operation Center at ROB. Some pre-defined operating modes are implemented in a so-called 'instrument manager': a sun–centered acquisition state with redundancy or not, a calibration state with either LED type on, and a standby state for the night part of the orbit. For flat-field evaluation, the platform will regularly perform a special sequence of off-pointings. Few non-routine activities are intended with the intervention of the ground operators.

Its high cadence is a scientific asset of LYRA, but it generates some non-negligeable amount of data. To reduce the telemetry, the on-board 'data manager' reorganizes the acquired data and compresses them losslessly. To make the scheme robust the time-lines are interleaved in three groups, so as to distribute contiguous records in separate packets.

3 Science Preparation

The span of LYRA Science is large; its reviewing is out of the scope of this paper. We present in this section some dedicated studies meant to feedback on the development decisions, and to prepare the timely exploitation of our instrument in view of its design.

3.1 Time series analysis and flares

The time series that will be recorded by LYRA can be modelled as the sum of a pure signal perturbed by some noise. Numerous tools have been developed in the statistical literature to analyse univariate (one-channel) or multivariate (multi-channel) time series. In our case, we aim at objectively providing a level of confidence to the detection of flares, whether small or not. We want to also establish correspondances between blips appearing in the four different wavebands.

Flares appear as 'peaks' in the time series. To detect these peaks, we use the multiscale approach of Bigot (2003a,b) that relies on the maxima of a continuous wavelet transform. This algorithm also produces *the structural intensity function*, that gives the importance of the flare detected. This quantity is continuous, as opposed to the threshold that are used nowadays to determine

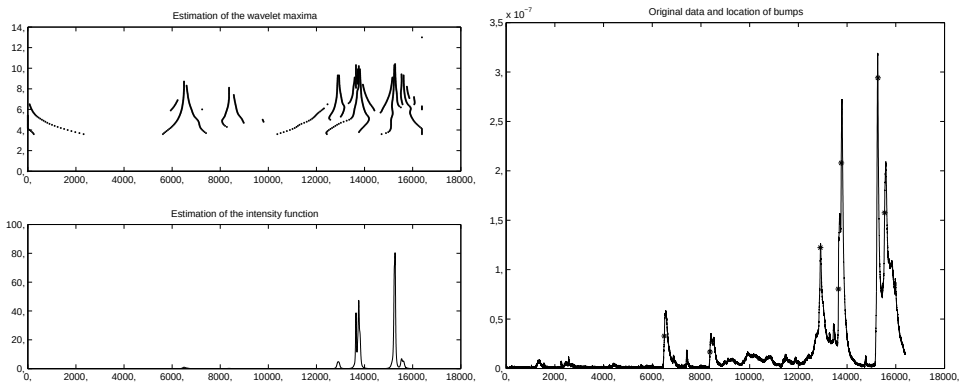

Fig. 4. Detection of peaks in the GOES data of February 9, 2001, in the 0.5-4 $\dot{A}$ waveband. (a) Maxima lines in the CWT (top). Structural intensity function (b) Stars '*' indicate the location of events detected.

the category of the flares (C-flare, M-flare, X-flare). As an illustration, Fig. 4 shows the analysis of one GOES X-ray time series using the algorithm developed by Bigot. After having detected the important events, it will be useful to link the four times series. One possibility is to *align* the curves using a registration method. Bigot (2003a) has proposed such a registration method based on the alignement of *landmarks* —characteristic features of the signal. Work in this direction is in progress.

3.2 Irradiance modelling and interplay with SWAP

A set of LYRA data may be used to compute a differential emission measure (DEM), which would enable the calculation of irradiances in individual optically thin spectral lines, also outside the spectral range of LYRA, using the equation

$$I_{\mathrm{k}} = \int_0^\infty G_{\mathrm{k}}(T)\zeta(T)\mathrm{d}T, \tag{1}$$

where $\zeta(T)$ denotes the DEM and the function $G_{\mathrm{k}}(T)$, dependent on temperature T, comprises the elemental abundance and the contribution function for the transition identified by the index k for the respective ion. $G(T)$ is in principle known for any optically thin line from theoretical calculations. Thus if the DEM is known, line irradiances for unobserved lines can be predicted.

Direct inversion of Eq. 1 is troublesome, since the problem is ill–contrained and the solution not unique. The situation gets worse if only a few lines at few formation temperatures can be measured. Often the DEM is then expressed in some functional form, mostly as a sum of Chebychev polynomials, ensuring a solution which resembles known well–measured DEMs. In case of LYRA,

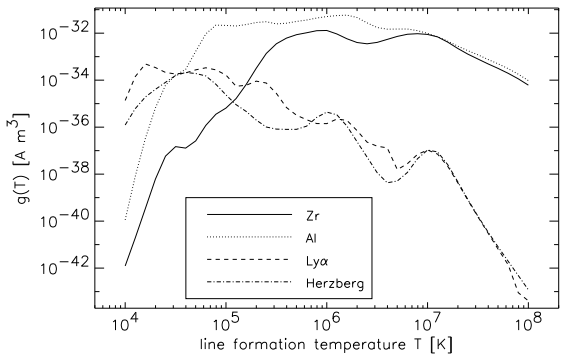

Fig. 5. Sum of line contribution functions, weighted with instrumental throughput (see Eq. 2). All lines from the CHIANTI database (Dere et al., 1997) enter the calculation, using solar coronal abundances from Feldman et al. (1992) and ionization equilibria from Arnaud and Rothenflug (1985); Arnaud and Raymond (1992); Landini and Fossi (1991). Note the units at the ordinate: prior to any calibration, the LYRA signal is given in Amperes per Watt, thus the units of the function $g(T)$ are Amperes $\times$ m^3.

the situation is even more complicated, not only because there are only four measurements at hand, but also because LYRA does not measure individual spectral lines but the sum of many lines of various formation temperatures and wavelengths within the wavelength range of each of the four bandpasses. Moreover, contributions from contiuum radiation and from optically thick lines for which Eq. 1 does not apply have to be corrected for.

Eq. 1 will apply for a LYRA measurement $I_{\mathrm{k}=1,2,3,4}$ after replacing the functions $G_{\mathrm{k}'}$ with

$$g_{\mathrm{k}}(T) = \sum_{\mathrm{k}'} F_{\mathrm{k}'\mathrm{k}} G_{\mathrm{k}'}(T), \qquad k = 1, 2, 3, 4. \tag{2}$$

The index k now denotes the four LYRA bandpasses, whereas the index for line transitions is replaced by k'. The summation runs over all optically thin lines k' within the LYRA bandpasses. $F_{\mathrm{k}'\mathrm{k}}$ denotes the response of the LYRA channel k at the wavelength of the transition k'. $F_{\mathrm{k}} = F_{\mathrm{k}}(\lambda)$ results from the known filter transmittances and detector responses. Ideally, the four LYRA channels could be designed in such a way that the four functions g peak at well distinct formation temperatures over the range of interest to ensure a well defined DEM. For instance, a comb–filter could pick out all relevant lines in some narrow range of formation temperature. In practise, however, one is restricted to the possibilities of filter and detector technology, and a best compromise has to be found. Fig. 5 shows the four functions $g_{\mathrm{k}}(T)$, suggesting that a sufficiently distinct temperature coverage is given in the range between $4 \lesssim \log(T) \lesssim 6$.

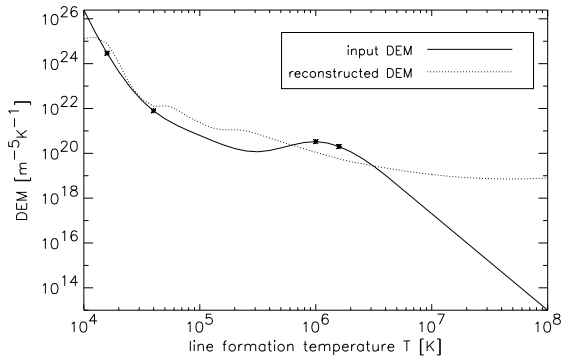

Fig. 6. Reconstruction of a DEM (dotted line) based on LYRA data constructed from an input DEM of the quiet Sun (solid line). The dots mark the temperature values which maximize the contribution functions to the four LYRA channels.

We found the best method to calculate the DEM to be an iteration scheme originally proposed by (Withbroe, 1975) and later refined by (Sylwester et al., 1980). Fig. 6 shows the result after 100 iteration steps of a DEM reconstruction to artificial LYRA data calculated on the basis of a DEM for the quiet Sun. While the reconstructed DEM reproduces the LYRA data within less than 1%, the DEM itself does not satisfactorily resemble the input DEM. This is due to the non-uniqueness of the solutions for Eq 1. No reproduction of the input DEM could be expected for temperatures above $\approx 10^6$ K, as the functions g in Eq. 5 are too ambiguous in that domain. The reconstruction around the two higher temperature values is also not as desired, due to the fact that the g functions do not peak very clearly at these temperatures. As a result, the reconstructed DEM seems to be averaged out. Only in the domain of cooler transitions does the fit approach the original DEM. It should be possible to enforce a better agreement by demanding a certain functional form resembling known DEMs, and iteratively fit such a form to agree with the input data.

An approach similar to the one used for the NRLEUV model (Warren et al., 2001) will take advantage of the availability of the SWAP telescope next to LYRA. In this way we hope as well to automatically recognize in SWAP the temporal features identified in LYRA. Work in these directions is in progress.

3.3 Aeronomy

Direct Sun observation from space allows the implementation of the *limb occultation* technique, a major tool in atmospheric remote sounding. The main advantage of the occultation mode lies in the derivation of an absolute quantity (the slant path optical thickness τ) from a relative measurement. Indeed, the determination of the atmospheric transmittance along the optical path is obtained as the ratio of the measured spectrum through the atmosphere by the

exo-atmospheric spectrum. Consequently, the measurement is not depending on the calibration of the detector. Orbital sunsets and sunrise, as seen from LYRA, are equivalent to a vertical scan of the atmosphere. For a circular orbit at 630 km of altitude, the vertical velocity of the tangent point is about 2.35 km/s, which means that the recording of the Sun occultation lasts about 65 seconds from 200 km down to 50 km. At the highest cadence (10 ms), the vertical distance between two acquisitions is about 25 m, a very favourable vertical sampling. The retrieval of an extinction profile from occultation data usually processes through a tandem of mathematical inversions: the spectral inversion consists of separating the contributions of different absorbers (O_2, Rayleigh) by using their respective cross sections; the vertical inversion is the numerical scheme by which the relative contributions of different atmospheric layers are extracted from the integrated column densities to produce a vertical concentration profile. In many occultation experiments, this last step is often performed by the well known "onion-peeling" technique. This is clearly not applicable for Lyra because the full solar disk (that spans about 25 km at the tangent point) is observed. At first sight, the apparent vertical resolution is of the same order of magnitude. But the true resolution that can be finally obtained will actually be positively influenced by the high signal-to-noise (SNR) ratio. Indeed, between two successive acquisitions, there is a large overlap between the respective solar disks, that could induce ill-conditioning in the inversion process. However, the high SNR clearly allows to differentiate the resulting signal in a much better vertical resolution. Dedicated inversion algorithms have been successfully applied in the past to the ORA occultation radiometer onboard the European Retrievable Carrier (EURECA) satellite (Fussen et al., 2000, 2001). In the 200–220 nm range, the mesospheric oxygen concentration profile is a clear scientific target via the photoabsorption by the X-A Herzberg continuum. The most significant altitude domain ranges from 100 km ($\tau \approx 0.001$) down to 50 km ($\tau \approx 2$). Although the 200–220 nm channel is located on the tail of the Hartley band ($\sigma = 5.10^{-19}\ cm^2$), the mesospheric ozone is still detectable ($\tau \approx 0.2$ at 60 km) in competition with molecular (Rayleigh) scattering. The second ozone maximum at 90 km should be detected at the edges of the instrument accuracy ($\tau \approx 0.002$). In the mesosphere-thermosphere, water vapour is photolyzed by the Lyman–α, leading to a considerable hydrogen production. Apart from an estimation of the water concentration profile, the large cross section ($10^{-17}\ cm^2$) should allow the detection of polar mesospheric clouds (PMC) which are thought to reflect the delayed perturbations of the stratospheric environment. In particular, the polar satellite orbit has a limited geographical coverage but is almost ideal for the detection of PMCs at high latitudes during a few weeks before and after solstice in the summer hemisphere. Lyman–α is also useful for molecular oxygen absorption in the Schumann-Runge continuum. Molecular nitrogen dominates atmospheric absorption in the extreme-ultraviolet spectral region for wavelengths immediately below 100 nm. N_2 shields the Earth's surface from XUV-EUV radiation through photodissociation, photoexcitation

and photoionization processes, in which the excited states play significant roles. These processes occur predominantly in the upper atmospheric layers above 100 km. Between 1 and 70 nm, effective extinction cross-sections will be constructed that incorporate all relevant ionic and atomic transitions (N,O). Also, depending on the final detector sensitivity, the nightglow could be be observed in the shadow of the Earth. Along with SWAP, STEREO/SECCHI and other EUV solar monitoring experiments, LYRA will be an effective instrument to study the impact of solar activity on conditions of the Earth's atmosphere.

4 Conclusions

The design, status and objectives of the LYRA instrument have been reviewed. The LYRA team will keep on preparing actively this mission to maximize its expected success in all regards.

Acknowledgements

The development of the LYRA instrument is funded by the Belgian Federal Science Policy Office (BELSPO), through the ESA/PRODEX programme. LYRA receives development support from its Swiss and German Co-Investigator institutions PMOD and MPS.. The LYRA team acknowledges the contribution of a very agreeable consortium.

During the preparation of this paper, we have learnt the sudden death of Pierre Cugnon. He was the department head of the ROB Solar Physics department, but also a dear friend and a colleague of several of the authors. We dedicate the solar payload of Proba 2 to the memory of Pierre Cugnon.

References

Arnaud, M., Raymond, J., Oct. 1992. Iron ionization and recombination rates and ionization equilibrium. ApJ 398, 394–406.

Arnaud, M., Rothenflug, R., Jun. 1985. An updated evaluation of recombination and ionization rates. A&AS 60, 425–457.

Bailey, S. M., Woods, T. N., Barth, C. A., Solomon, S. C., Canfield, L. R., Korde, R., Dec. 2000. Measurements of the solar soft X-ray irradiance by the Student Nitric Oxide Explorer: First analysis and underflight calibrations. J. Geophys. Res. , 27179–27194.

Ben Moussa, A., Schühle, U., Haenen, K., Neslàdek, N., Koizumi, S., Hochedez, J.-F., 2004. PIN Diamond Detector Development for LYRA, the Solar VUV radiometer on Board PROBA–2. Physica Status Solidi (a) .

Ben Moussa et al, A., 2005. Solarblind diamond detector for LYRA, the Solar VUV radiometer on Board PROBA–2. Submitted to Experimental Astronomy .

Berghmans, D., 2005. SWAP, the Sun watcher using APS detector on-board PROBA-2. Submitted to ASR .

Bigot, J., 2003a. Automatic landmark registration of 1d curves. In: Akritas, M., Politis, D. (Eds.), Recent advances and trends in nonparametric statistics . Elsevier, to appear.

Bigot, J., 2003b. Recalage de signaux et analyse de variance fonctionnelle par ondelettes. applications au domaine biomédical. Ph.D. thesis, Université Joseph Fourier , Grenoble, France.

Brueckner, G. E., Edlow, K. L., Floyd, L. E., Lean, J. L., Vanhoosier, M. E., Jun. 1993. The solar ultraviolet spectral irradiance monitor (SUSIM) experiment on board the Upper Atmosphere Research Satellite (UARS). J. Geophys. Res. 98, 10695–+.

Defise, J., Berghmans, D., Hochedez, J. E., Lecat, J. M., Mazy, E., Rochus, P. L., Thibert, T., Nicolosi, P., Pelizzo, M. G., Schühle, U. H., Van der Linden, R. A. M., Zhukov, A. N., Feb. 2004. SWAP: Sun watcher using APS detector on-board PROBA-2, a new EUV off-axis telescope on a technology demonstration platform. In: Telescopes and Instrumentation for Solar Astrophysics. Edited by Fineschi, Silvano; Gummin, Mark A. Proceedings of the SPIE, Volume 5171, pp. 143-154 (2004). . pp. 143–154.

Dere, K. P., Landi, E., Mason, H. E., Monsignori Fossi, B. C., Young, P. R., Oct. 1997. CHIANTI - an atomic database for emission lines. A&AS 125, 149–173.

Egorova, T., Rozanov, E., Manzini, E., Haberreiter, M., Schmutz, W., Zubov, V., Peter, T., Mar. 2004. Chemical and dynamical response to the 11-year variability of the solar irradiance simulated with a chemistry-climate model. Geophys. Res. Lett. 31, 6119–+.

Feldman, U., Mandelbaum, P., Seely, J. F., Doschek, G. A., Gursky, H., Jul. 1992. The potential for plasma diagnostics from stellar extreme-ultraviolet observations. ApJS 81, 387–408.

Fussen, D., Vanhellemont, F., Bingen, C., Feb. 2001. Remote Sensing of the Earth s Atmosphere by the Spaceborne Occultation Radiometer, ORA: Final Inversion Algorithm. Appl. Opt. 40, 941–948.

Fussen, D., Vanhellemont, F., Bingen, C., Chabrillat, S., Nov. 2000. Ozone profiles from 30 to 110 km measured by the Occultation RAdiometer instrument during the period Aug 1992-Apr 1993. Geophys. Res. Lett. 27, 3449–3452.

Greenhough, J., Chapman, S. C., Dendy, R. O., Nakariakov, V. M., Rowlands, G., Oct. 2003. Statistical characterisation of full-disk EUV/XUV solar irradiance and correlation with solar activity. A&A 409, L17–L20.

Hochedez, J., Lemaire, P., Pace, E., Schühle, U., Verwichte, E., Sep. 2001. Wide bandgap EUV and VUV imagers for the Solar Orbiter. In: ESA SP-493: Solar encounter. Proceedings of the First Solar Orbiter Workshop . pp. 245–250.

Hochedez, J. E., Schühle, U. H., Pau, J. L., Alvarez, J., Hainaut, O., Appourchaux, T. P., Auret, F. D., Belsky, A., Bergonzo, P., Castex, M. C., Deneuville, A., Dhez, P., Fleck, B., Haenen, K., Idir, M., Kleider, J. P., Lefeuvre, E., Lemaire, P., Monroy, E., Muret, P., Munoz, E., Nesladek, M., Omnes, F., Pace, E., Peacock, A. J., Van Hoof, C. A., Feb. 2003a. New UV detectors for solar observations. In: Innovative Telescopes and Instrumentation for Solar Astrophysics. Edited by Stephen L. Keil, Sergey V. Avakyan . Proceedings of the SPIE, Volume 4853 . pp. 419–426.

Hochedez, J.-F., Appourchaux, T., Belsky, A., Castex, M. C., Deneuville, A., Dhez, P., Fleck, B., Hainaut, O., Idir, M., Kleider, J.-P., Lemaire, P., Monroy, E., Munoz, E., Muret, P., Nesladek, M., Omnes, F., Pau, J.-L., Peacock, A., Schühle, U., van Hoof, C., Jun. 2003b. Imageur diamant et nitrures pour l'observation UV du soleil. Journal de Physique IV 108, 227–231.

Hochedez, J.-F., Schühle, U., Lemaire, P., 2002. New UV Detector Concepts. In: The Radiometric Calibration of SOHO, ISSI Scientific Report SR-002. Edited by A. Pauluhn, M.C.E. Huber and R. von Steiger. ESA Publications Division, Noordwijk, The Netherlands . pp. 371–+.

Hochedez, J.-F., Verwichte, E., Bergonzo, P., Guizard, B., Mer, C., Tromson, D., Sacchi, M., Dhez, P., Hainaut, O., Lemaire, P., Vial, J.-C., 2000. Future Diamond UV Imagers For Solar Physics. Physica Status Solidi Applied Research 181, 141–149.

Judge, D. L., McMullin, D. R., Ogawa, H. S., Hovestadt, D., Klecker, B., Hilchenbach, M., Möbius, E., Canfield, L. R., Vest, R. E., Watts, R., Tarrio, C., Kühne, M., Wurz, P., 1998. First Solar EUV Irradiances Obtained from SOHO by the CELIAS/SEM. Sol. Phys. 177, 161–173.

Koizumi, S., Watanabe, K., Hasegawa, M., Kanda, H., Jun. 2001. Ultraviolet Emission from a Diamond pn Junction. Science 292, 1899–1901.

Landini, M., Fossi, B. C. M., Nov. 1991. Ion equilibrium for minor components in a thin plasma. A&AS 91, 183–196.

Lean, J. L., Warren, H. P., Mariska, J. T., Bishop, J., Feb. 2003. A new model of solar EUV irradiance variability 2. Comparisons with empirical models and observations and implications for space weather. J. Geophys. Res.(Space Physics) 108, 2–1.

Mitrofanov, A. V., Apel, P. Y., Oct. 1989. Porous plastic membranes used as extreme and far ultraviolet radiation diffraction filters. Nuclear Instruments and Methods in Physics Research A 282, 542–545.

Newmark, J. S., Cook, J. W., McMullin, D. R., May 2001. Solar EUV Variability as Measured by SOHO/EIT: Comparison to SOHO SEM and He II 304, Case Studies. AGU Spring Meeting Abstracts , 32–+.

Remes, Z., Petersen, R., Haenen, K., Neslàdek, M., 2005. Mechanism of pho-

toconductivity in intrinsic epitaxial CVD diamond studied by photocurrent spectroscopy and photocurrent decay measurements. Diamond and Related Materials .

Rottman, G. J., Woods, T. N., Sparn, T. P., Jun. 1993. Solar-Stellar Irradiance Comparison Experiment 1. I - Instrument design and operation. J. Geophys. Res. 98, 10667–+.

Rozanov, E. V., Schlesinger, M. E., Egorova, T. A., Li, B., Andronova, N., Zubov, V. A., Jan. 2004. Atmospheric response to the observed increase of solar UV radiation from solar minimum to solar maximum simulated by the University of Illinois at Urbana-Champaign climate-chemistry model. J. Geophys. Res.(Atmospheres) 109, 1110–+.

Schühle, U. H., Hochedez, J. E., Pau, J. L., Rivera, C., Munoz, E., Alvarez, J., Kleider, J., Lemaire, P., Appourchaux, T., Fleck, B., Peacock, A., Richter, M., Kroth, U., Gottwald, A., Castex, M., Deneuville, A., Muret, P., Nesladek, M., Omnes, F., John, J., Van Hoof, C., Feb. 2004. Development of imaging arrays for solar UV observations based on wide band gap materials. In: Telescopes and Instrumentation for Solar Astrophysics. Edited by Fineschi, Silvano; Gummin, Mark A. Proceedings of the SPIE, Volume 5171 . pp. 231–238.

Snow, M., McClintock, W., Rottman, G., Woods, T. N., May 2004. Solar Flares in the UV from SORCE SOLSTICE. AGU Spring Meeting Abstracts , A4+.

Sylwester, J., Schrijver, J., Mewe, R., Sep. 1980. Multitemperature analysis of solar X-ray line emission. Sol. Phys. 67, 285–309.

Teston, F., Creasey, R., Bermyn, J., K., M., Aug. 1999. PROBA: ESAs Autonomy and Technology Demonstration Mission. In: Proceedings of the 13th Annual AIAA/USU, Conference on Small Satellites .

Vanhoosier, M. E., Bartoe, J.-D. F., Brueckner, G. E., Prinz, D. K., Cook, J. W., 1981. A high precision Solar Ultraviolet Spectral Irradiance Monitor for the wavelength region 120-400 NM. Sol. Phys. 74, 521–530.

Wang, H., Qiu, J., Denker, C., Spirock, T., Chen, H., Goode, P. R., Oct. 2000. High-Cadence Observations of an Impulsive Flare. ApJ 542, 1080–1087.

Warren, H. P., Mariska, J. T., Lean, J., Aug. 2001. A new model of solar EUV irradiance variability: 1. Model formulation. J. Geophys. Res. , 15745–15758.

Withbroe, G. L., Dec. 1975. The analysis of XUV emission lines. Sol. Phys. 45, 301–317.

Woods, T., Jun. 2002. Solar vacuum ultraviolet irradiance measurements and models for solar cycle 23. In: ESA SP-508: From Solar Min to Max: Half a Solar Cycle with SOHO . pp. 165–172.

Woods, T., Eparvier, F., Woodraska, D., Dec. 2003. Solar Ultraviolet Variability During the TIMED Mission. AGU Fall Meeting Abstracts , B2+.

Woods, T. N., Bailey, S. M., Eparvier, F. G., Lawrence, G. M., Lean, J., McClintock, W. E., Roble, R. G., Rottman, G. J., Solomon, S. C., Tobiska, W. K., Ucker, G. J., White, O. R., Nov. 1998. TIMED solar EUV experiment. In: Proc. SPIE Vol. 3442, p. 180-191, Missions to the Sun II, Clarence

M. Korendyke; Ed. . pp. 180–191.

Woods, T. N., Eparvier, F. G., Fontenla, J., Harder, J., Kopp, G., McClintock, W. E., Rottman, G., Smiley, B., Snow, M., May 2004. Solar irradiance variability during the October 2003 solar storm period. Geophys. Res. Lett. 31, 802–+.

Woods, T. N., Rottman, G. J., Ucker, G. J., Jun. 1993. Solar-Stellar Irradiance Comparison Experiment 1. II - Instrument calibrations. J. Geophys. Res. 98, 10679–+.